Journal of Physics: Conference Series **530** (2014) 012059 doi:10.1088/1742-6596/530/1/012059

Stress field analysis around vortex in elastic layer of viscoelastic turbulent channel flow

T Minegishi, T Tsukahara and Y Kawaguchi
Department of Mechanical Engineering, Tokyo University of Science
Yamazaki 2641, Noda, Chiba 278-8510, Japan

E-mail: tlvkrl@gmail.com

Abstract. It is important from an engineering aspect to understand drag-reducing viscoelastic flow, since comprehension of the drag-reduction mechanism may facilitate designs with better additive types and/or channel configurations. In this study, we investigated the attenuation of vortices in fully-developed turbulence of viscoelastic fluid between parallel planes by DNS (Direct Numerical Simulation). We discussed how the viscoelastic stress play a role in the reduction of the turbulent motions around vortices and how it influences the entire flow field. For determining the major effect of viscoelasticity, we classified three stages of vortex evolution and examined statistical data for each stage. We clarified the relation between the velocity field and viscoelastic stress field using a product, or a correlation, between vorticity and rotational viscoelastic stress. We found that the inhibition of turbulence would be caused by the following aspects: damping longitudinal vortex by viscoelastic stress over a wide range in the channel, and relaxing development of vortex by the stress in vortex growing state.

1. Introduction

Viscoelastic fluid flows appear in chemical plants, food industries, and other industrial applications. In turbulent flows of dilute surfactant or water-soluble polymer solutionsthat provide viscoelasticity to the fluid,we may find the suppression of turbulent frictional drag, the so-called Toms effect.Viscoelastic fluid, with which we may obtain a high energy savings at low cost, is expected to be one promising way to solve energy issues.

There are many studies on drag-reduced wall turbulence of viscoelastic fluids by experiments and direct numerical simulations (DNS): see, for example, [1-5]. Dimitropoulos et al. [6] concluded that the large extensional viscosity of a viscoelastic fluid inhibited longitudinal vortices in turbulence, based on the budgets of the Reynolds stresses obtained by DNS. Kim &Sureshkumar [7] demonstrated developments/attenuations of a hairpin vortex localized in a viscoelastic fluid flow and found the self-consistent evolution of the vortex.However, the dynamics of vortex in the viscoelastic turbulent flow has not been sufficiently elucidated nor evaluated statistically.There are few studies of vortices by a statistical approach, despite many researches in the Newtonian flow [8-10].

In this study, we numerically investigated stress fields around vortices in viscoelastic flow through a channel. Especially, we focused on an elastic layer that should be absent in the Newtonian flow. In the elastic layer, an additional force originating from the fluid viscoelasticity would be expected to affect vortices significantly with either enhancing or attenuating the fluid vortical motions.

2. Numerical method

2.1. Governing equation and parameter

In this study, we adopted DNS, which may allow us to extract stress fields and fine-scale vortices. The governing equations for the calculation are

- the equation of continuity

$$\frac{\partial u_i^+}{\partial x_i^*} = 0 \tag{1}$$

- the momentum equation

$$\frac{\partial u_i^+}{\partial t^*} + u_j^+ \frac{\partial u_i^+}{\partial x_j^*} = -\frac{\partial p^+}{\partial x_i^*} + \frac{\beta}{\mathrm{Re}_\tau}\frac{\partial u_i^+}{\partial x_j^* \partial x_j^*} + \frac{1-\beta}{\mathrm{We}_\tau}\frac{\partial c_{ij}}{\partial x_j^*} \tag{2}$$

- the viscoelastic constitutive equation based on the Giesekus model

$$\frac{\partial c_{ij}}{\partial t^*} + u_k^+ \frac{\partial c_{ij}}{\partial x_k^*} - c_{ik}\frac{\partial u_j^+}{\partial x_k^*} - c_{jk}\frac{\partial u_i^+}{\partial x_k^*} + \frac{\mathrm{Re}_\tau}{\mathrm{We}_\tau}\left[\alpha\left(c_{ij}-\delta_{ij}\right)^2 + \left(c_{ij}-\delta_{ij}\right)\right] = 0 \tag{3}$$

where c_{ij} is the conformation tensor, $\mathrm{Re}_\tau=\rho u_\tau \delta/\mu_0$ is the frictional Reynolds number, $\mathrm{We}_\tau=\rho u_\tau^2 \lambda/\mu_0$ is the frictional Weissenberg number, α is the mobility factor for the Giesekus model, and $\beta=\mu_s/\mu_0$ is the ratio of the solvent contribution to the total zero-shear viscosity. Here, ρ is the solution density, u_τ is the frictional velocity, δ is the channel half height, λ is the relaxation time, $\mu_0=\mu_a+\mu_s$ is the zero-shear viscosity of the solution, μ_a is the zero-shear viscosity of the solvent, and μ_s is the zero-shear viscosity of the solvent.The quantities with superscript (+) indicate the wall-unit normalization by u_τ, and (*) represents the outer-scale normalization by δ.The streamwise, wall-normal, and spanwise direction are labeled as x_1, x_2 and x_3 direction, respectively.

For the spatial discretization, the finite difference method was applied. We chose the Giesekus model as the constitutive equation to compute c_{ij}. In order to improve numerical stability, we employed the minmod flux-limiter scheme, which exhibited good numerical stability and accuracy, to the advection term in equation (3). The detailed information of numerical scheme we used here can be found in our previous paper [4]. Table 1 shows numerical parameters and conditions in this work.

Table 1. Numerical parameters: Δt is the time step; L_i and N_i are the computational domain size and the number of grids in i direction, respectively.

Re_τ	We_τ	α	β	Δt^+	$L_1\times L_2\times L_3$	$N_1\times N_2\times N_3$
395	30	0.001	0.5	0.0079	$12.8\delta\times 2\delta\times 6.4\delta$	$512\times 192\times 256$

2.2. Method of vortex extraction

In this section, we briefly introduce methods for extracting vortices and averaging them. Let us use y_s^+ as a wall-normal distance of the x_1-x_3 plane we focus, and $Q2=-u_{i,j}^+ u_{j,i}^+$ a vortex strength based on the second invariant of the velocity-gradient tensor.To reduce numerical oscillation, we used $\overline{Q2}^w$ as the weighted and averaging (or filtered) $Q2$. Figure 1 shows an example of $\overline{Q2}^w$ distribution in a horizontal plane at $y_s^+=25$, where one may see a spike (at C_1) corresponding to a vortex center. Here, the point C_1, at which $\overline{Q2}^w$ is a local minimum and larger than a threshold value $Q2^T$, was defined as the vortex center. The strength of the extracted vortex at C_1 is quantified by C_{Q2}, and its temporal gradient is defined as $A = \partial C_{Q2}/\partial t^+$. Based on A, we determined the state of vortex of interest. The values of those thresholds ($Q2^T$ and A) are shown in table 2.

Table 2. Control parameters for vortex extraction.

y_s^+	12.5	25	40
$A_u(=-A_d)$	0.0077	0.0077	0.0059
$Q2^T$	0.0034	0.038	0.0038

In this study, we divided the vortex states into 3 stages: that is, a growing state of vortex, $A \geq A_u$; a sustaining state, $A_d \leq A < A_u$; and a damping state, $A \leq A_d$). It should be noted that A_u was determined to satisfy the following equation:

$$\frac{\int_{A_d}^{A_u} P(A)}{\int_{-\infty}^{+\infty} P(A)} = 0.8, \tag{4}$$

where$P(A)$ is the probability density function (PDF) of A.

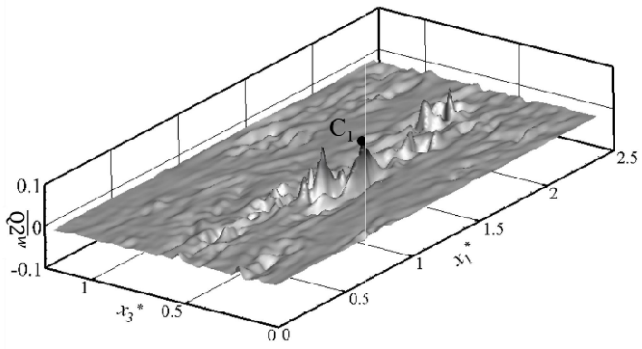

Figure 1. Distribution of in the x_1-x_3 plane at x_2^+= 25. The point of C_1 indicates the centre of a vortex. A part of the computation domain is shown. The mean flow moves from bottom-left to top-right.

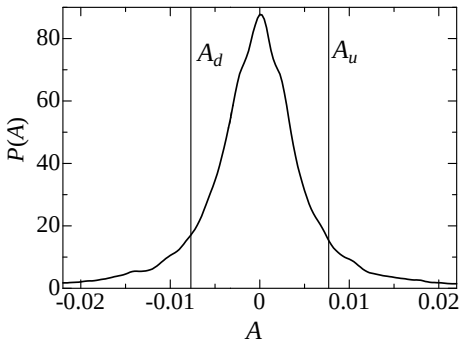

Figure 2. The probability density function of temporal gradient of vortex strength at the centre of vortex at x_2^+= 25. By criteria A_u and A_d, the state of vortex is classified.

3. States of vortex evolution

Figure 3 shows a time series of C_{Q2} at a vortex center in the viscoelastic turbulent channel flow. Here, the vortex we arbitrary chose and focused is labelled as 'V1'. It can be seen from the figure that the vortex sustained itself for a while after its development. The time range of $0 \leq t^+ < 7$ where we find a comparatively large increase in $C_{Q2}(A \geq A_u)$ is named as 'the growing state'; the plateau region corresponds to 'the sustaining state' for $7 \leq t^+ < 12$; and the range with a monotonic decrease in $C_{Q2}(A < A_d)$ is called as 'the damping state'after t^+ = 12. Moreover, G (t^+=4.0), C (t^+=8.3), and D (t^+=15.8) are defined as the instants corresponding to the median of individual state.

Figures 4 and 5 show instantaneous field at the instants of G, C and D, which are visualized from the spanwise direction. In the figures, the abscissa is the streamwise direction and the ordinate is the wall-normal direction.Gray iso-surfaces indicate vortices visualized by $Q2$. Red/blue contour shows the magnitude (or the correlation) of $\omega_i^+ \omega_{Ei}^+$, which is a production of the vorticity $\omega_i^+ = \varepsilon_{ijk} u_{k,j}^+$ and the rotational viscoelastic stress $\omega_{Ei}^+ = \varepsilon_{ijk} c_{kl,jl}$. Here, ε_{ijk} describes the Levi-Civita symbol. In a region where $\omega_i^+ \omega_{Ei}^+$ is negative, the viscoelastic stress is exerting on the vortical motion. The contour of $\omega_1^+ \omega_{E1}^+$ presents the viscoelastic contributions around streamwise vortices. In figure 4, $\omega_1^+ \omega_{E1}^+$ is found to be negative near the wall, indicating that the viscoelastic stress would inhibit longitudinal vortices in the near-wall region. The vortex V1, which is the strongest vortex in the focused area shown in figure 4,

seems to be large with time, because the viscoelastic stress works on the vortex and would suppress its vertical motion.

Figure 5 shows the viscoelastic contribution with respect to the spanwise component $\omega_3^+\omega_{E3}^+$. The distribution of $\omega_3^+\omega_{E3}^+$ reveals that the viscoelastic stress affects the shear (or the vortex sheet) rather than the vortex. We conjecture that the viscoelastic stress would prevent occurrence of ejection from the near-wall region by relaxing the high-shear layer between relatively high-speed and low-speed regions.

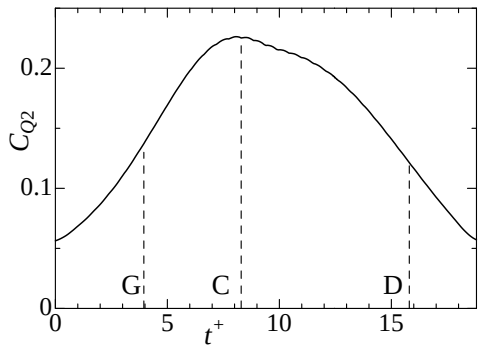

Figure 3. A time variation of a vortex V1 at y_s^+=25 (G, the growing state of vortex; C, the sustaining state; and D, the damping state).

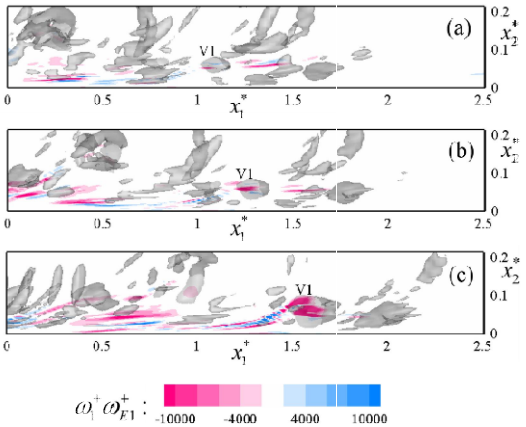

Figure 4. Time variation of vortices: the mean flow moves to right. Gray iso-surfaces, positive $Q2$ regions corresponding to vortices; colour contour, $\omega_1^+\omega_{E1}^+$. (a) at the growing state, G; (b) the sustaining state, C; and (c) the damping state, D.

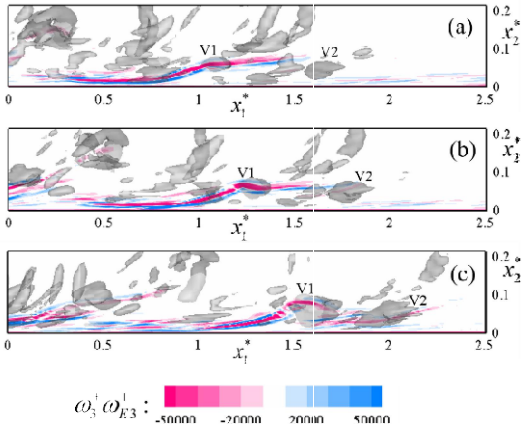

Figure 5. Same as figure 4, but the colour contour shows $\omega_3^+\omega_{E3}^+$.

4. Statistical investigation

Figures 6-8 show statistical fields, which are acquired by the conditional averaging described in section 2.2. The contours show either or . Figures 6(a) and 7(a) show the growing state of the vortex with its center at y_s^+ = 25, (b) the sustaining state, (c) the damping state.

The distribution of shown in figure 6 reveals that the streamwise vortex encounters the resistance force of the viscoelastic stress. This aspect is similarly found in each distribution given in figure 6, implying less dependency on the wall-normal height. However, the relatively small magnitude of at the reference point (the vortex center) in figure 6(c) means the less correlation between the vortical motion and the reaction of viscoelastic stress. As can be seen from the figures, the

negative correlation between them becomes significant in the near-wall region irrespectively of the wall-normal position of vortex.

In figure 7, the contours of in the near-wall region reveals sheet-like distribution. As found in the instantaneous field (figure 5), the viscoelastic stress works against the high shear region. Similar inclined structure of the high regions are observed in both figures 5(a) and 7(a). Thus, it can be said that the viscoelastic stress would relax high-shear layer on the growing state of a near-wall vortex. On the other hand, the viscoelastic stress has rather small influence on the vortex at the sustaining and damping states: see figures 7(b) and (c).

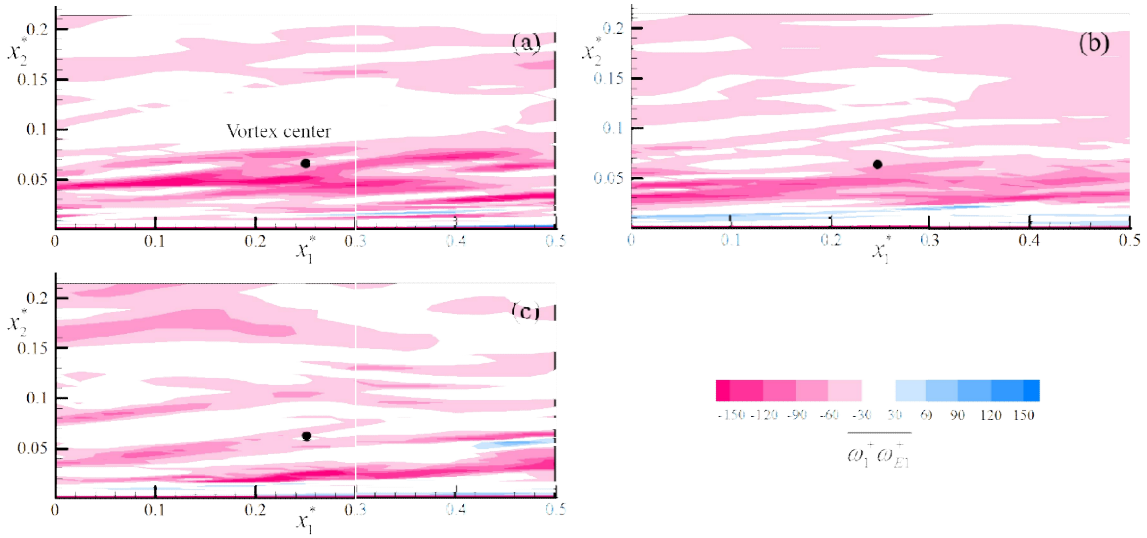

Figure 6. The difference of vortex state by streamwise rotational viscoelastic contribution in statistic field at y_s^+=25. (a) growing state of vortex; $A \geq A_u$, (b) conservation state; $A_d \leq A < A_u$, and (c) damping state; $A \leq A_d$.

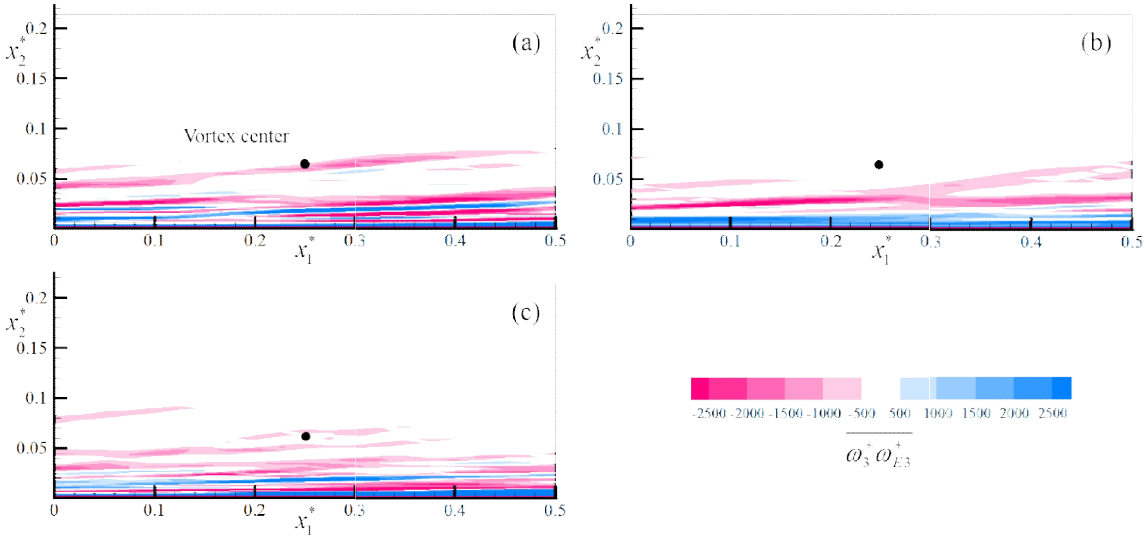

Figure 7. The difference of vortex state by spanwise rotational viscoelastic contribution in statistic field at y_s^+=25. (a) growing state of vortex; $A \geq A_u$, (b) conservation state; $A_d \leq A < A_u$, and (c) damping state; $A \leq A_d$.

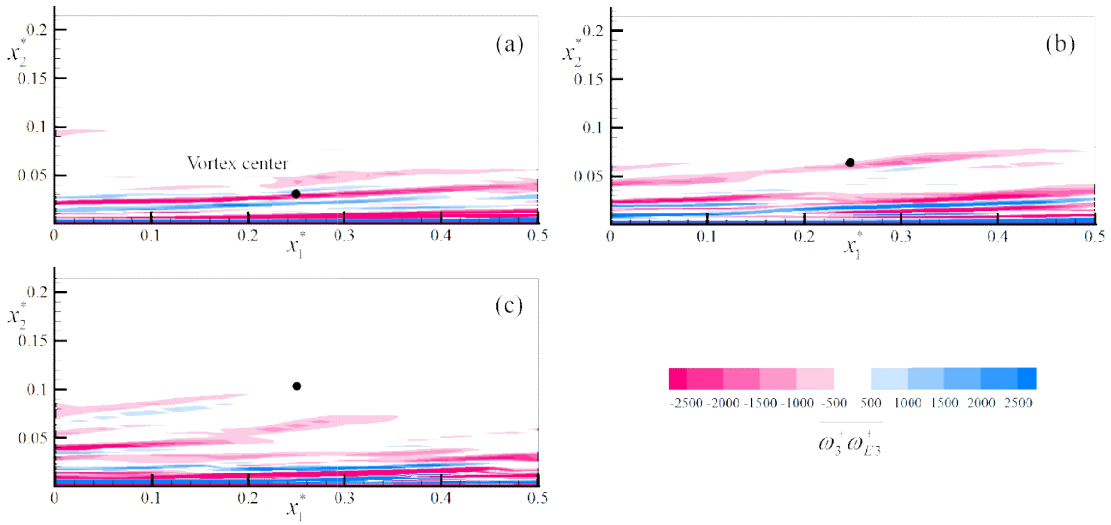

Figure 8. Dependence of the spanwise rotational viscoelastic contribution in on y_s^+ at the growing state. (a) y_s^+=12.5, (b) y_s^+=25, and (c) y_s^+=40.

Figure 8 shows the contours of for the growing state with comparing results with different reference heights (y_s^+=12.5, 25, and 40). The viscoelastic stress contribution relaxes shear layers in x_2^+<30. This near-wall layer may relate to the elastic layer, which is absent in the Newtonian flow. The mean velocity profile (figure not shown) indicates the elastic layer appears in $7 \leq x_2^+ \leq 30$ in the present flow condition.

5. Conclusions

We investigated the viscoelastic contribution around vortices, based on the correlation of the vorticity and the rotational viscoelastic stress, in a viscoelastic turbulent channel flow. For determining the major effect of viscoelastic stress, we examined statistical data, with emphasis on the vortex evolution. We found that viscoelastic stress would relax high-shear layers in the growing state of a vortex. As a result, viscoelastic stress prevent occurring to ejection. Moreover, the longitudinal vortex tends to be reduced by the viscoelastic stress throughout the channel. In the viscoelastic flow, turbulent motions would be inhibited by these two factors: the suppressions of high shear and of developing streamwise vortex.

6. References

[1] Virk P S 1971 *J. Fluid Mech.***45** 417
[2] Dimitropoulos C D, Sureshkmar R and Beris A N 1998 *J. Non-Newtonian Fluid Mech.***79** 433
[3] Yu B, Li F and Kawaguchi Y 2004 *Int. J. Heat and Fluid Flow***25** 961
[4] Tsukahara T, Ishigami T, Yu B and Kawaguchi Y 2013*J. Turbulence***12** N13
[5] Thais L, Gatski T B and Mompean G 2013*Int. J. Heat and Fluid Flow***43** 52
[6] Dimitropoulos C D, Suresukmar R, Beris A N and Handler R A 2001 *Phys. Fluids***13** 1016
[7] Kim K and Sureshkmar R 2013 *Phys. Rev. E* **87** 063002
[8] Jeong J, Hussain F, Schoppa W and Kim J 1997 *J. Fluid Mech.***332** 185
[9] Zhou J, Adrian R J, Balachander S and Kendall T M 1999 *J. Fluid Mech.***387** 353
[10] Adrian R J 2007 *Phys. Fluid***19** 041301
[11] Kasagi N, Sumitani Y, Suzuki Y and Iida O 1995 *Int. J. Heat and Fluid Flow***16** 2-10

Acknowledgments
This work was supported by Grants-in-Aid for Scientific Research (C) #25420131 from Japan Society for the Promotion of Science (JSPS). The present DNS was performed using the super supercomputing resources at CyberscienceCenter, Tohoku University, and at CybermediaCenter, Osaka University.